Electronic Supplementary Information

Atomic-layered Pt clusters on S-vacancy rich MoS$_{2-x}$ with enhanced electrocatalytic hydrogen evolution activity

Feng Shi,[#a,b] Wenzhuo Wu,[#a,b] Jiafu Chen,[*a] Qun Xu[*a,b]

[a]College of Materials Science and Engineering, Zhengzhou University, Zhengzhou 450052, P.R. China. * e-mail: chenjf@zzu.edu.cn; qunxu@zzu.edu.cn
[b]Henan Institute of Advanced Technology, Zhengzhou University, Zhengzhou, 450052 P. R. China.

Experimental section

Chemicals and materials

The MoS$_2$ powder was purchased from Sigma-Aldrich. H$_2$PtCl$_6$ · 6H$_2$O, NaBH$_4$, HCl, H$_2$SO$_4$ and ethanol used were purchased from Sinopharm Chemical Reagent Co., Ltd. (China) and used without further treatment. Pt/C (20 wt.%) and Nafion solution (5 wt.%) were obtained from Sigma-Aldrich. Nitogen and Argon with a purity of 99.999% was provided by the Zhengzhou Shuangyang Gas Co. and used as received. Deionized (DI) water with a resistivity of 18.2 MΩ•cm was prepared via a Milli-Q Water Purification System.

Synthesis of Sv-MoS$_{2-x}$ nanosheets.

The production of Sv-MoS$_{2-x}$ nanosheets was carried out through the previously reported solid-phase reduction process using NaBH$_4$ as reductant. Typically, 2 g NaBH$_4$ and 1 g bulk MoS$_2$ was mixed through sufficient grinding. Then the mixture was put into the furnace, blow with high-purity nitrogen at 60 °C for 30 min, and heated at 330 °C for 2 h. After cooling down to room temperature, the mixture was added slowly into a flask with 4M HCl solution and vigorously stirred for 5 hours. After that, the mixture was washed by water for several times till the supernatant liquid turned cloudy after high-speed (10000 rpm) centrifugation. Then the dispersion was centrifuged at 5000 rpm for 30 mins to remove aggregates. Finally, the product in supernatant was washed by water and ethanol and was separated after a high-speed centrifugation and drying in a vacuum oven.

Synthesis of Pt/Sv-MoS$_{2-x}$ catalyst

A wetness impregnation method which an appropriate amount of H$_2$PtCl$_6$ · 6H$_2$O was loaded onto the Sv-MoS$_{2-x}$ support was used to synthesize Pt/Sv-MoS$_{2-x}$ catalyst. Typically, 20 mg Sv-MoS$_{2-x}$ nanosheets prepared as previous was dissolved in 10 mL mixture of deionized water and ethanol (Volume ratio ,1:1) to form a homogeneous solution. Then, amount of 46.6 mM L^{-1} H$_2$PtCl$_6$ 6H$_2$O aqueous solution was added into the above-mentioned solution dropwise under stirring. The solvent was keeping stirring at room temperature for 4 hours. Consequently, evaporate the solvent in a vacuum oven at 50 °C overnight. The precipitates were grinded into power and annealed in a tubular furnace under flowing Ar (100 mL min^{-1}) to a target temperature of 300 °C with ramping rate of 5 °C min^{-1}, keeping for 4 h. All catalysts

with different loading ratios were obtained by the same method as above. The Pt content was not separately measured because there is no chance that Pt would be lost during the synthesis. Therefore, we used the target value when catalysts were prepared for every batch.

Characterization

The morphology and elemental mapping images of the samples was measured by using a transmission electron microscopy (TEM) FEI TalosF200S. The HAADF-STEM images were taken using FEI Tecnai G2 F20 S-TWIN operating at 200 kV. X-Ray diffraction (XRD) patterns of the samples were collected on a Rigaku D/Max 2550 X-ray diffractometer with Cu Kα radiation (λ= 1.5418 Å). Raman analysis was carried out on an inVia Raman spectrometer (LabRAM HR Evo, FRA) with 532nm Single Frequency CW Solid State Laser. Electron paramagnetic resonance (EPR) experiment with a BRUKER EMX plus-9.5/12/P/L electron spin resonance spectrometer was carried out at room temperature. The X-ray photoelectron spectroscopy (XPS) measurements were performed on an XPS, ESCA Lab250 X-ray photoelectron spectrometer (Thermo Fisher Scientific, USA) with Al Kα source. All XPS spectra were corrected using C 1s line at 284.6 eV, and curve fitting and background subtraction were accomplished.

Electrochemical measurements

All the electrochemical experiments were implemented in a three-electrode system with an electrochemical station (CHI760E, Shanghai Chenhua Instrument Factory, China). The working electrode was a glassy carbon electrode (diameter 3 mm). Platinum wire and Ag/AgCl (saturated KCl-filled) electrode were served as counter and reference electrodes, respectively. All measurements were performed in N_2-saturated 0.5 M H_2SO_4 aqueous solution (PH=0.47). For HER experiments, 4.0 mg catalyst was ultrasonically dispersed for 30 min in 2 mL ethanol containing 0.1 wt% Nafion, and 7 μL of homogeneous catalyst ink was then transferred onto the glassy carbon electrode with a geometric area of 0.0706858 cm^2. The catalyst loading was 0.2 mg cm^{-2}. The linear sweep voltammograms (LSVs) and cyclic voltammograms (CVs) were measured at a scan rate of 2 mV s^{-1} in 0.5 M H_2SO_4 solution. 5%Pt/Sv-MoS$_{2-x}$ and 20% Pt/C drop-casted on carbon paper for large current densities measurements and tested under the same conditions.

Cyclic voltammetry (CV) curves were measured under different scan rates (10, 20, 40, 60, 80, 100 and 120 mV s^{-1}). These data were used to calculate the

electrochemical double-layer capacitance (C_{dl}). In addition, the HER activity at large current densities up to 1000mA cm^{-2} was measured on the carbon paper (0.5 cm × 0.5 cm) with the same measurement condition. Prior to measurement, several fast CV scans (50 mv s^{-1}) between 0 and -0.6 v (vs. RHE) were applied to remove the surface contaminants and electrochemical activate the sample until a stable voltammogram curve was obtained. All potentials used in this work have been converted to the RHE scale.

$$E(vs.RHE) = E(vs.Ag/AgCl) + 0.197 + 0.0592 \times PH$$

The kinetic parameter TOF is defined as

$$TOF(s^{-1}) = (J * A)/2 * F * n$$

Where J is the current density (C s^{-1} cm^{-2}) at a given overpotential, A is the surface area of the electrode (cm^2), F is the Faraday constant (96485.4 C mol^{-1}), the factor ½ is the number of electrons required to make one hydrogen molecule, and n is the molar mass of the active metal component.

The directory of abbreviate names

P-MoS$_2$: Pristine MoS$_2$ without the soild phase reduction through NaBH$_4$.

Sv-MoS$_{2-x}$: MoS$_2$ nanosheets with lots of sulfur vacancies through the NaBH$_4$ thermal treatment.

5%Pt/P-MoS$_2$: Pristine MoS$_2$ with the 5% Pt species loaded.

5%Pt/Sv-MoS$_{2-x}$: Sv-MoS$_{2-x}$ with the 5% Pt species loaded.
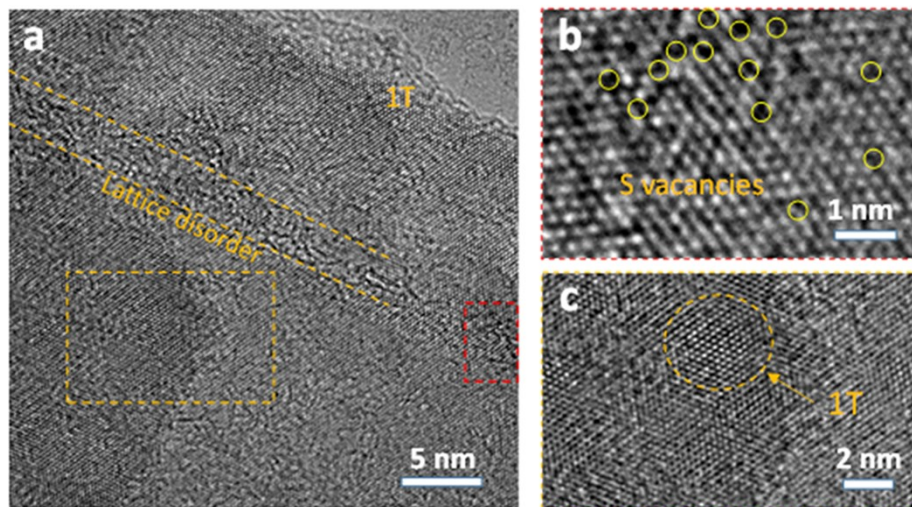
Supporting Results

Fig. S1. (a) The HRTEM image of Sv-MoS$_{2-x}$ nanosheets. (b) and (c) are enlarged images corresponding to the red and orange boxes in (a), respectively. The lattice disorder, large area of S vacancies and 1T phase transformation on the Sv-MoS$_{2-x}$ nanosheets can be observed.
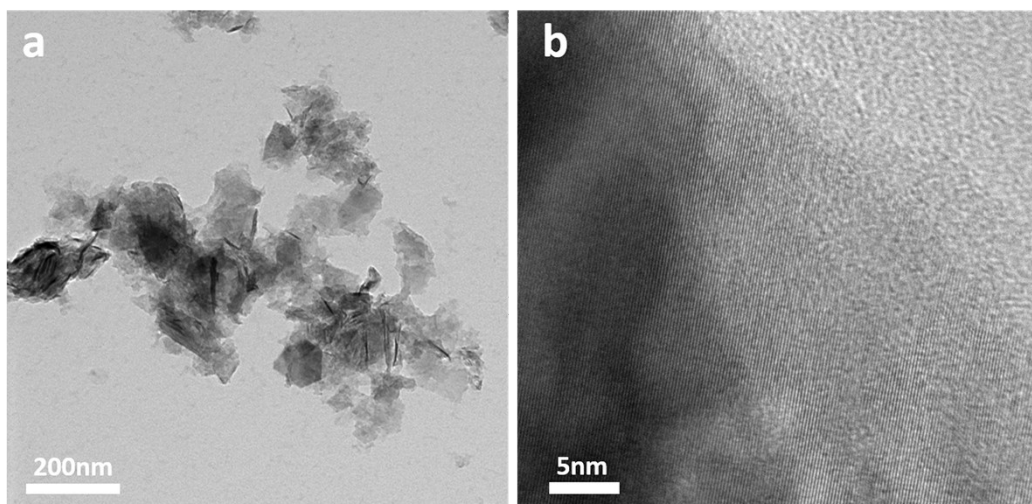
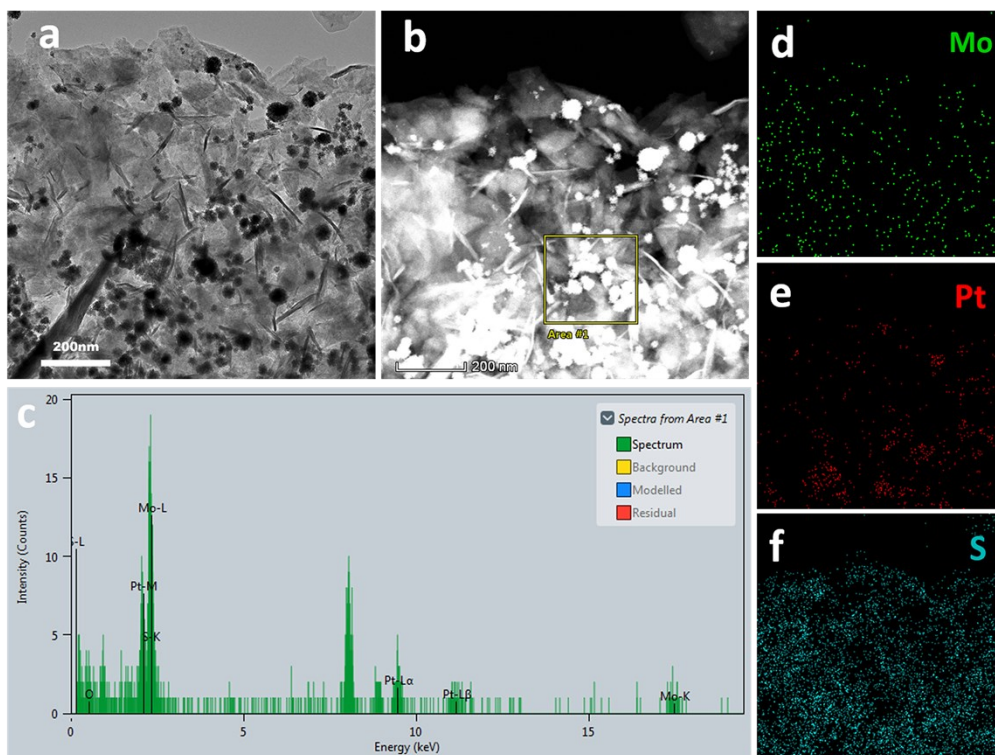**Fig. S2.** (a) TEM and (b) HRTEM images of as-prepared Sv-MoS$_{2-x}$ supports.

Fig. S3. The TEM image (a) and correspond HAADF image (b) of 5%Pt/P-MoS$_2$ samples without sulfur vacancies. (c)The EDS results and (d-f) elements mappings of the regions filtered by the yellow curve in (b). As shown in the pictures above, Pt particles supported on P-MoS$_2$ nanosheets tend to aggregate together with size larger than 20 nm, which are dramatically different with Pt clusters on Sv-MoS$_{2-x}$, indicating the necessity of S vacancy for stabilizing Pt clusters.
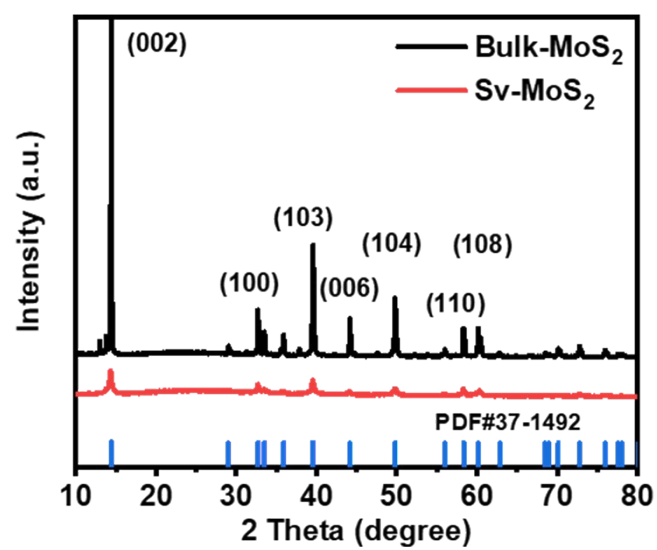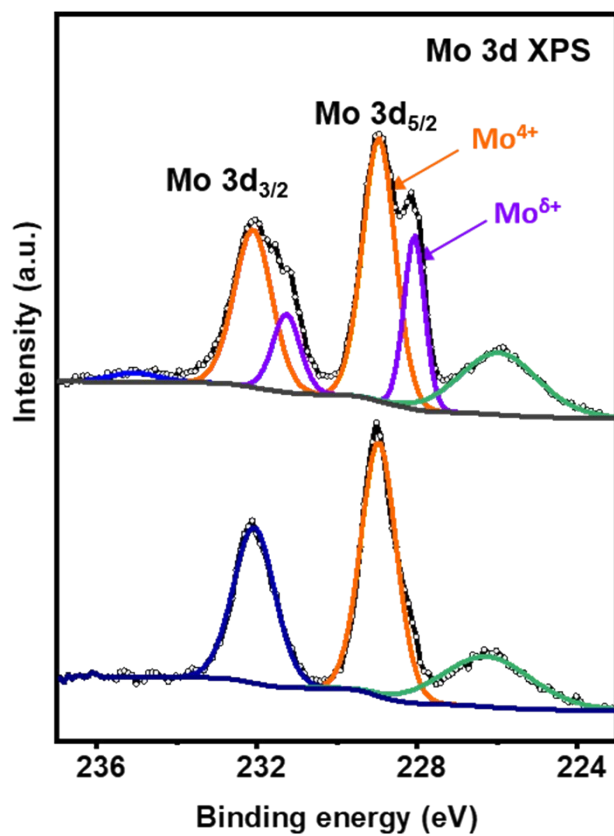
Fig. S4. XRD pattern of bulk MoS_2 and Sv-MoS_{2-x}.

Fig. S5. High-resolution Mo 3d core-level XPS spectra of bulk MoS_2 and Sv-MoS_{2-x} nanosheets.

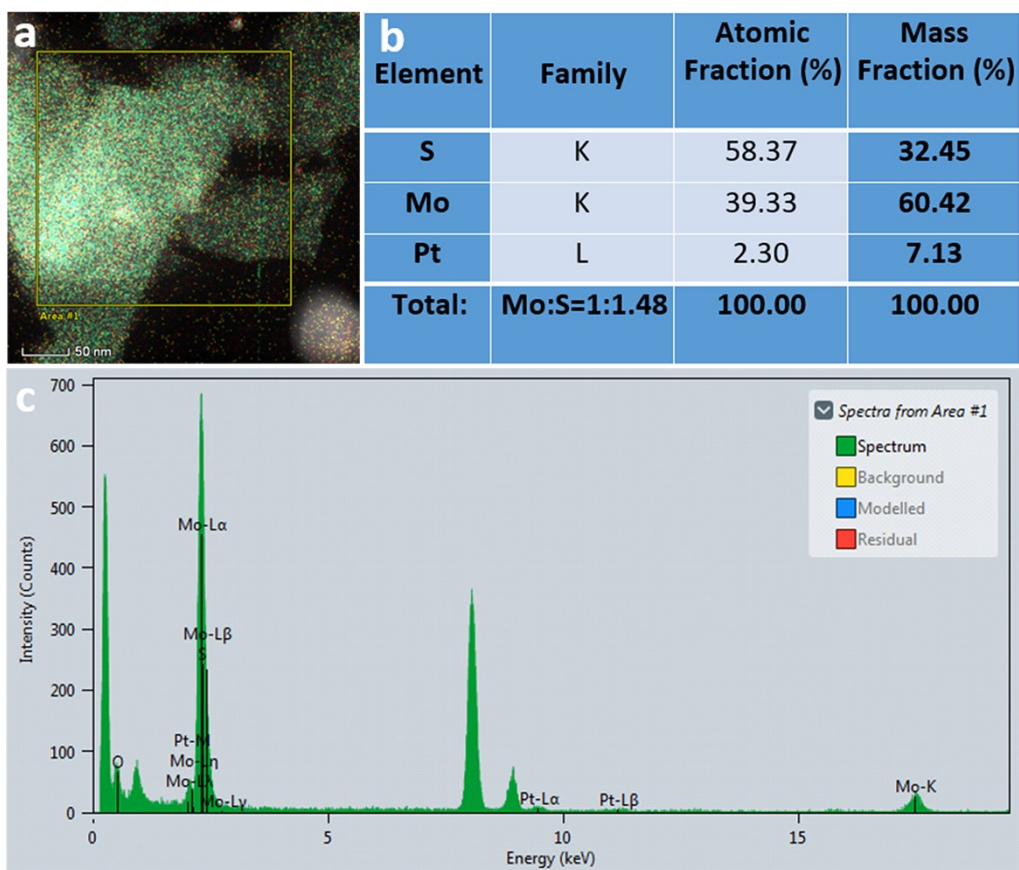| Element	Family	Atomic Fraction (%)	Mass Fraction (%)
S	K	58.37	32.45
Mo	K	39.33	60.42
Pt	L	2.30	7.13
Total:	Mo:S=1:1.48	100.00	100.00

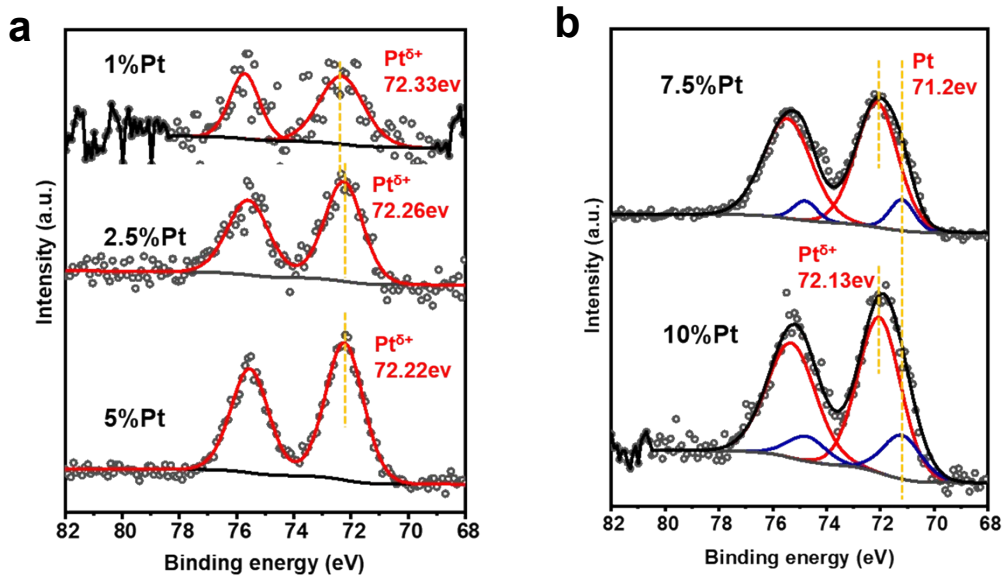**Fig. S6.** The EDS analysis results of 5%Pt/Sv-MoS$_{2-x}$ nanosheets.

Fig. S7. High-resolution Pt 4f core-level XPS spectra of Pt/Sv-MoS$_{2-x}$ samples with different Pt loading mass. The Pt$^{\delta+}$ ($0 < \delta < 4$) peaks are located between those of Pt^0 and Pt^{4+}, indicating that the Pt atoms on Sv-MoS$_{2-x}$ surface possess more positive valence state than those in Pt nanoparticles. Such a partial charged state can be attributed to the strong interaction between Pt and the adjacent Mo atoms exposed on the supports. This resulted from a charge redistribution and manipulated the electronic and geometric structure of Pt species on Sv-MoS$_{2-x}$.
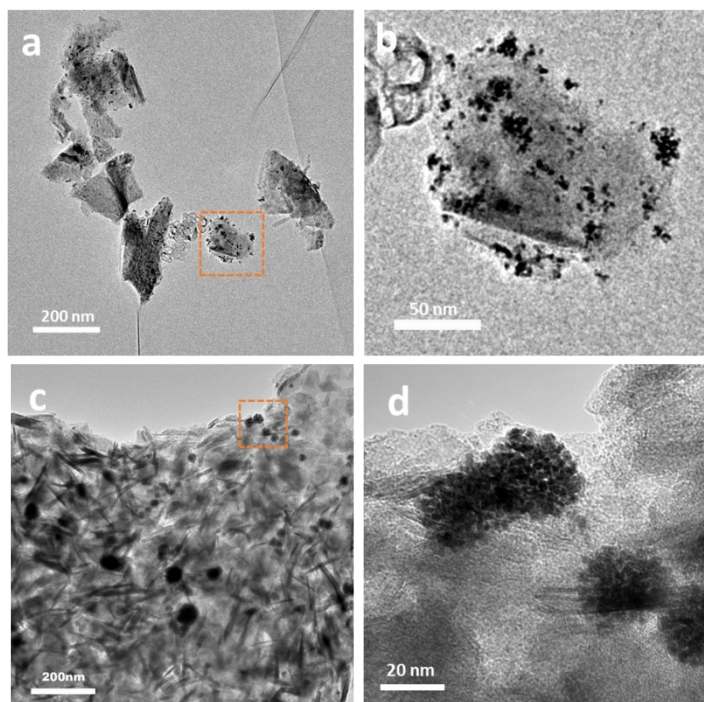
Fig. S8. (a)The TEM images of 7.5%Pt/Sv-MoS$_{2-x}$ nanosheets and (b) the enlarged image corresponding to the orange curves filtered in (a). (c) The TEM images of 10%Pt/Sv-MoS$_{2-x}$ nanosheets and (d) the enlarged image corresponding to the orange curves filtered in (c). It can be found that there are black Pt particles appearing on the Sv-MoS$_{2-x}$ nanosheets.
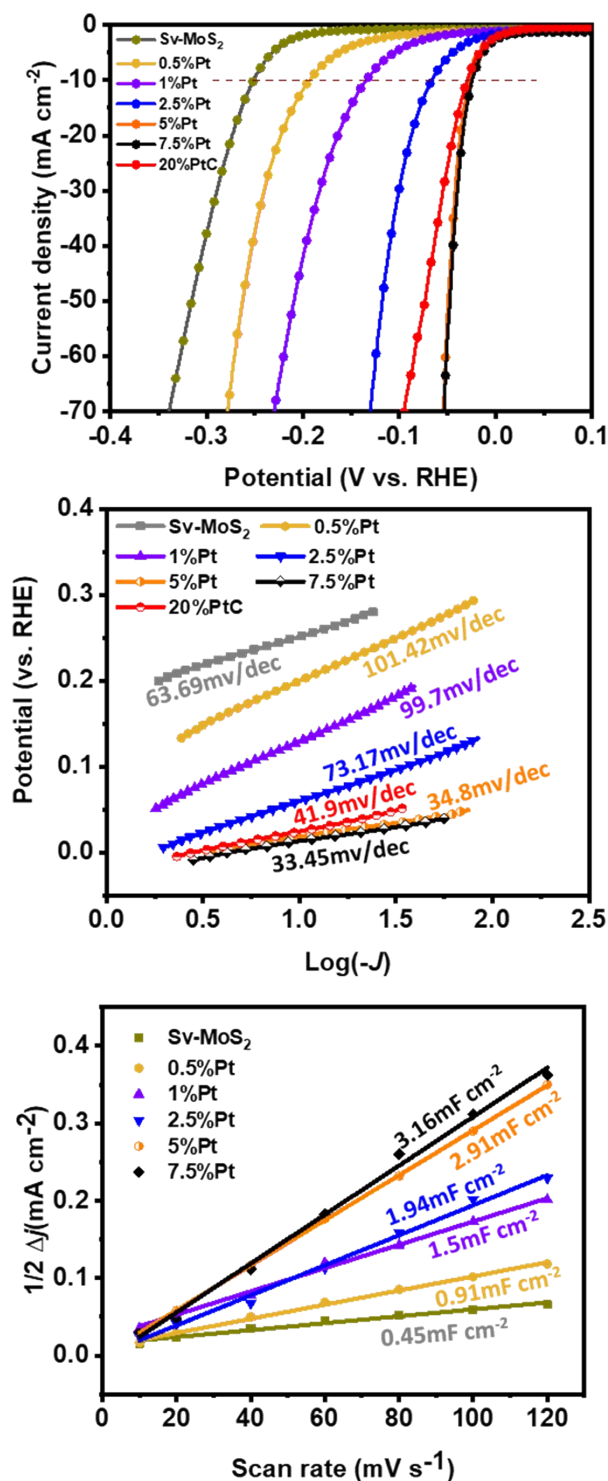
Fig. S9. The controlled trials to identify the optimal Pt loadings in the electrocatalysis process. (a) The LSV curves and overpotentials at 10 mA cm^{-2} of Pt/Sv-MoS$_{2-x}$ (0.5-7.5%), Sv-MoS$_{2-x}$, commercial 20% Pt/C catalysts, respectively. The Sv-MoS$_{2-x}$ exhibits the poorest HER activity with a 253 mv overpotential at 10 mA cm^{-2}, and the HER catalytic performance are gradually increasing as long as thein creasing of loading Pt mass. Notably, the HER performance of catalysts tends to stagnate when the Pt contents reach to7.5%, which might due to the self-aggregation when

overloaded (Figure S8). (b) Tafel plots of different Pt mass loading samples. The tafel slope of 5%Pt/Sv-MoS$_{2-x}$ is as low as 34.8 mV dec^{-1}, indicating that the HER mechanism abides the Volmer-Tafel reaction pathway. (c) C$_{dl}$ curves of different samples. The C$_{dl}$ values of different mass loadings Pt/Sv-MoS$_2$ nanosheets increased to from 0.91 mF cm^{-2} for the 0.5%Pt/Sv-MoS$_2$ to 3.16 mF cm^{-2} for the 7.5%Pt/Sv-MoS$_{2-x}$ nanosheets, obviously higher than the value of 0.45 mF cm^{-2} for Sv-MoS$_{2-x}$. The results indicate that the electrochemically active surface areas can be tuned through the decoration of Pt.
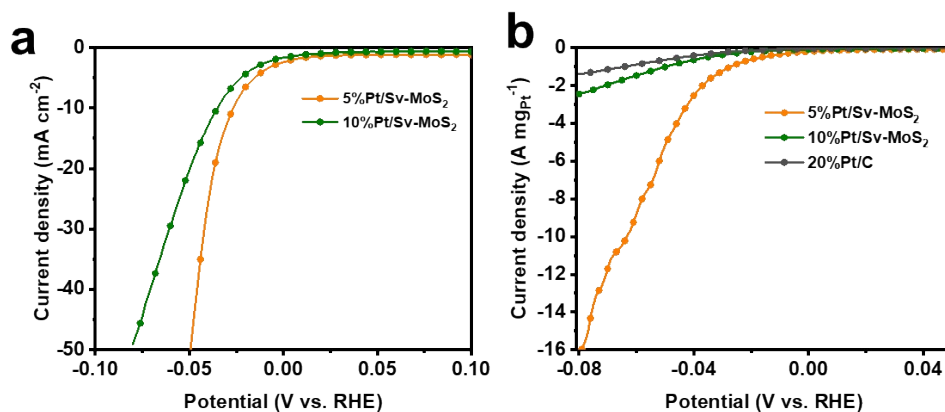
Fig. S10. (a) The LSV curves of 5%Pt/Sv-MoS$_{2\text{-x}}$ and 10%Pt/Sv-MoS$_{2\text{-x}}$ samples. (b) Pt mass activities (normalized to Pt content) of 5%Pt/Sv-MoS$_{2\text{-x}}$, 10%Pt/Sv-MoS$_{2\text{-x}}$ and 20%Pt/C. Notably, the response mass activity (current/mg$_{Pt}$, normalizing to Pt content) of 5%Pt/Sv-MoS$_{2\text{-x}}$ (16.02 A mg$_{Pt}^{-1}$ at 80 mv) is 6.5 times higher than that of 10%Pt/Sv-MoS$_{2\text{-x}}$ (2.46 A mg$_{Pt}^{-1}$ at 80 mv) and 11 times higher than that of 20%Pt/C(1.44 A mg$_{Pt}^{-1}$ at 80 mv).
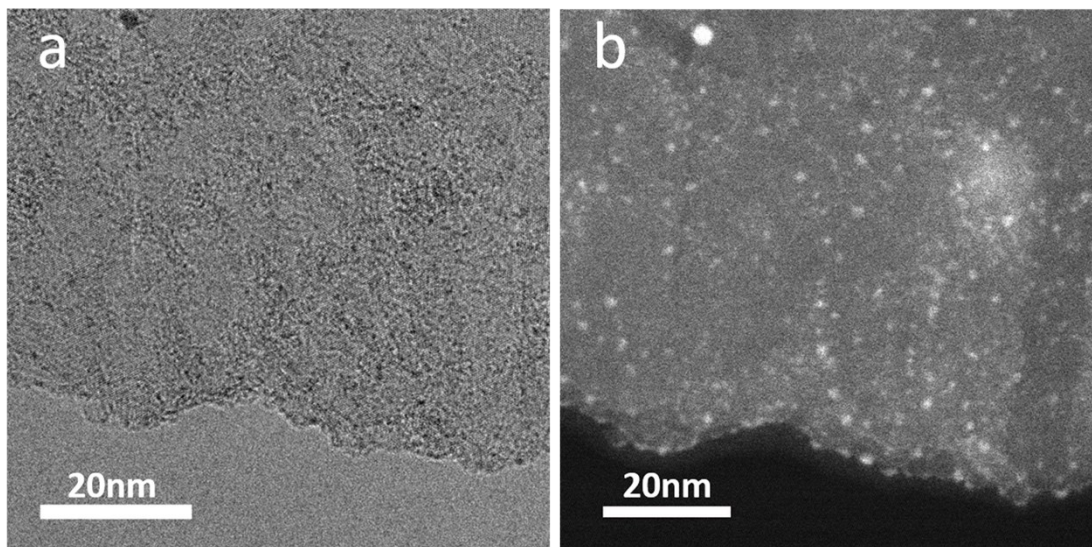
Fig. S11. (a) The HRTEM and (b) HAADF images of the used samples. The size of Pt clusters is unchanged, and no obvious Pt particles occurred in the images above, indicating the stability of as-prepared structure.
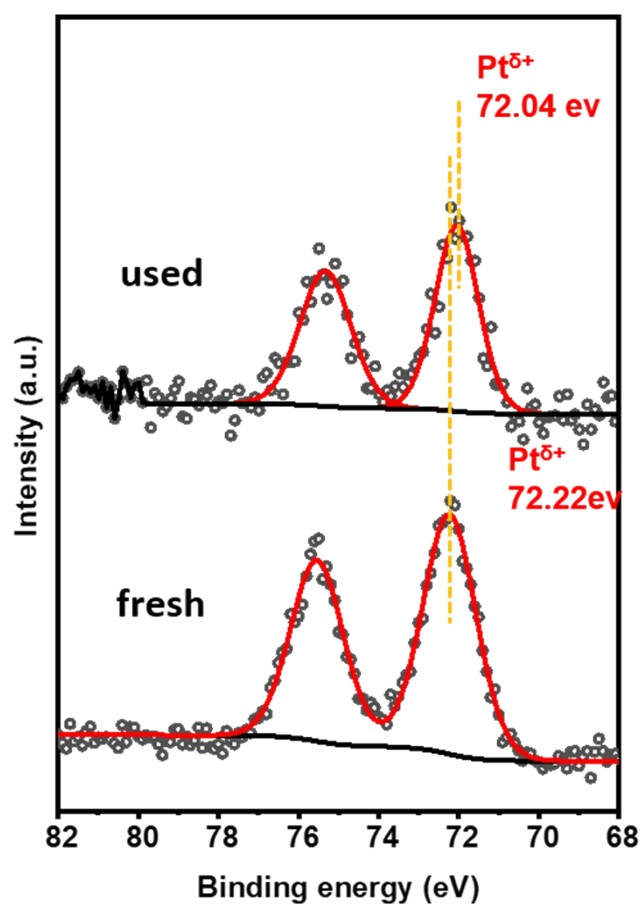
Fig. S12. High-resolution Pt 4f core-level XPS spectra of the 5%-Pt/Sv-MoS$_{2-x}$ before and after 1000 circles of CV test. There is no obvious shift of Pt 4f binding energy, indicating that the samples possess an excellent HER catalytic durability of Pt/Sv-MoS$_{2-x}$ in acidic solution.

Table S1. A summary of Pt-based catalysts for electrocatalytic HER in acidic media.

Catalyst	Overpotential 10 mA cm^{-2} (mV)	Mass activity (A mg$_{Pt}^{-1}$)	Reference
Pt/Sv-MoS$_{2-x}$	**26.6**	16.02 at 80 mV	This work
SA Pt-decorated VS$_2$	77	22.88 at 200 mV	Ref.[1]
Pt-MoS2	60	/	Ref.[2]
Pt-1T′ MoS$_2$	180	/	Ref.[3]
Pt$_1$/OLC	38	/	Ref.[4]
Pt/TiO$_2$-OVs	60	/	Ref.[5]
Pt$_1$/NMHCS	40	2.07 at 50 mV	Ref.[6]
Pt$_5$/HMCS‐5.08%	20.7	3.23 at 70mV	Ref.[7]
Pt-PVP/TNR@GC	21	16.53 at 50 mV	Ref.[8]
Pt@PCM	106	/	Ref.[9]
Pt$_1$@Fe-N-C	60	/	Ref.[10]
PtN$_x$/TiO$_2$	67	37.5 at 50 mV	Ref.[11]
Pt/f-MWCNTs	43.9	18.16 at 50 mV	Ref.[12]
Pt SASs/AG	12	22.4 at 50 mV	Ref.[13]
PtO$_x$/TiO$_2$	160	8.68 at 50 mV	Ref.[14]
PtTe$_2$-600 NSs	20	/	Ref.[15]
Pt/np-Co$_{0.85}$Se	55	1.32 at 100 mV	Ref.[16]

Reference

1. J. Zhu, L. Cai, X. Yin, Z. Wang, L. Zhang, H. Ma, Y. Ke, Y. Du, S. Xi, A. T. S. Wee, Y. Chai and W. Zhang, *ACS Nano*, 2020, **14**, 5600-5608.
2. J. Deng, H. Li, J. Xiao, Y. Tu, D. Deng, H. Yang, H. Tian, J. Li, P. Ren and X. Bao, *Energy Environ. Sci.*, 2015, **8**, 1594-1601.
3. C. Wu, D. Li, S. Ding, Z. u. Rehman, Q. Liu, S. Chen, B. Zhang and L. Song, *J. Phys. Chem. Lett.*, 2019, **10**, 6081-6087.
4. D. Liu, X. Li, S. Chen, H. Yan, C. Wang, C. Wu, Y. A. Haleem, S. Duan, J. Lu, B. Ge, P. M. Ajayan, Y. Luo, J. Jiang and L. Song, *Nat. Energy*, 2019, **4**, 512-518.
5. X. Cheng, Y. Lu, L. Zheng, M. Pupucevski, H. Li, G. Chen, S. Sun and G. Wu, *Mat. Today Energy*, 2021, **20**, 100653.
6. P. Kuang, Y. Wang, B. Zhu, F. Xia, C.-W. Tung, J. Wu, H. M. Chen and J. Yu, *Adv. Mater.*, 2021, 2008599.
7. X.-K. Wan, H. B. Wu, B. Y. Guan, D. Luan and X. W. Lou, *Adv. Mater.*, 2020, **32**, 1901349.
8. C. Li, Z. Chen, H. Yi, Y. Cao, L. Du, Y. Hu, F. Kong, R. Kramer Campen, Y. Gao, C. Du, G. Yin, I. Y. Zhang and Y. Tong, *Angew. Chem. Int. Ed.*, 2020, **59**, 15902-15907.
9. H. Zhang, P. An, W. Zhou, B. Y. Guan, P. Zhang, J. Dong and X. W. Lou, *Sci. Adv.*, 2018, **4**, eaao6657.
10. X. Zeng, J. Shui, X. Liu, Q. Liu, Y. Li, J. Shang, L. Zheng and R. Yu, *Adv. Energy Mater.*, 2018, **8**, 1701345.
11. X. Cheng, Y. Lu, L. Zheng, Y. Cui, M. Niibe, T. Tokushima, H. Li, Y. Zhang, G. Chen, S. Sun and J. Zhang, *Nano Energy*, 2020, **73**, 104739.
12. J. Ji, Y. Zhang, L. Tang, C. Liu, X. Gao, M. Sun, J. Zheng, M. Ling, C. Liang and Z. Lin, *Nano Energy*, 2019, **63**, 103849.
13. S. Ye, F. Luo, Q. Zhang, P. Zhang, T. Xu, Q. Wang, D. He, L. Guo, Y. Zhang, C. He, X. Ouyang, M. Gu, J. Liu and X. Sun, *Energy Environ. Sci.*, 2019, **12**, 1000-1007.
14. X. Cheng, Y. Li, L. Zheng, Y. Yan, Y. Zhang, G. Chen, S. Sun and J. Zhang, *Energy Environ. Sci.*, 2017, **10**, 2450-2458.
15. X. Li, Y. Fang, J. Wang, H. Fang, S. Xi, X. Zhao, D. Xu, H. Xu, W. Yu, X. Hai, C. Chen, C. Yao, H. B. Tao, A. G. R. Howe, S. J. Pennycook, B. Liu, J. Lu and C. Su, *Nat. Commun.*, 2021, **12**, 2351.
16. K. Jiang, B. Liu, M. Luo, S. Ning, M. Peng, Y. Zhao, Y.-R. Lu, T.-S. Chan, F. M. F. de Groot and Y. Tan, *Nat. Commun.*, 2019, **10**, 1743.